# Reproducibility of proton MR spectroscopic imaging findings.

G Tedeschi, A Bertolino, G Campbell, A S Barnett, J H Duyn, P K Jacob, C T Moonen, J R Alger and G Di Chiro

*AJNR Am J Neuroradiol* 1996, 17 (10) 1871-1879
http://www.ajnr.org/content/17/10/1871

# Reproducibility of Proton MR Spectroscopic Imaging Findings

G. Tedeschi, A. Bertolino, G. Campbell, A. S. Barnett, J. H. Duyn, P. K. Jacob, C. T. W. Moonen, J. R. Alger, G. Di Chiro

**PURPOSE:** To study the intraindividual, interindividual, and intraregional reproducibility of multisection proton MR spectroscopic imaging in healthy adults. **METHODS:** Six subjects were studied three times with proton MR spectroscopic imaging. Multisection long-echo-time proton MR spectroscopic imaging permits simultaneous acquisition of *N*-acetylaspartate (NAA), choline-containing compounds (Cho), and creatine plus phosphocreatine (Cr) signal intensities from four 15-mm-thick sections divided into 0.84-mL single-volume elements. Regions of interest were the frontal cortex, the occipital cortex, the parietal cortex, the insular cortex, the cingulate gyrus, the centrum semiovale, the thalamus, and the caudate. Statistical evaluation was performed by analyses of variance and components of variance method. **RESULTS:** The ratio NAA/Cr showed the lowest overall coefficient of variation (CV, %) in most of the regions of interest (range, 8.9 to 26.1). Interregional differences in the overall CV were present. Interindividual CVs ranged from 4.2 to 8.7 for NAA/Cr, from 6.8 to 17.4 for NAA/Cho, and from 5.0 to 13.6 for Cho/Cr. Intraindividual CVs ranged from 8.2 to 22.2 for NAA/Cr, from 12.8 to 25.8 for NAA/Cho, and from 4.5 to 21.0 for Cho/Cr. Intraregional CVs ranged from 12.3 to 21.2 for NAA/Cr, from 13.0 to 20.4 for NAA/Cho, and from 12.2 to 18.9 for Cho/Cr. **CONCLUSIONS:** Proton MR spectroscopic imaging showed good overall reproducibility. The finding of interregional variations of CV indicates that care is needed when using this imaging technique for follow-up studies.

**Index terms:** Brain, magnetic resonance; Efficacy studies; Magnetic resonance spectroscopy

*AJNR Am J Neuroradiol* 17:1871–1879, November 1996

The reproducibility of proton magnetic resonance (MR) spectroscopy and proton MR spectroscopic imaging observations in healthy control subjects is a key factor for establishing the reliability of longitudinal observations made on patients during disease progression or treatment. As with all scientific measurements, proton MR spectroscopic imaging observations will be influenced by a variety of factors that limit the ability to reproduce exactly measurements made at different times on different subjects. Of particular concern is the fact that proton MR spectroscopic imaging is characterized by a relatively low signal-to-noise ratio as compared with other methods. Moreover, pseudorandom factors like intersubject and interstudy differences in field homogeneity, subject positioning, and choice of volumes to be sampled could conceivably add further uncertainty to the observations. The regional distribution pattern of metabolite signal intensities in the brains of young adults by long-echo-time (TE) multisection proton MR spectroscopic imaging has recently been reported (1). Exploratory studies relevant to the reproducibility of multisection long-TE proton MR spectroscopic imaging in healthy control subjects have been done with the use of related proton MR spectroscopic techniques. Narayana et al (2) studied the repeatability of single-volume long-TE proton MR spectroscopy, and Jackson et al (3) studied the reproducibility of single-section short-TE proton MR spectroscopic imaging. The present

Received February 28, 1996; accepted after revision June 3.

From the Neuroimaging (G.T., A.B., A.S.B., P.K.J., G.D.) and the Biometry and Field Studies (G.C.) Branches, National Institute of Neurological Disorders and Stroke, the In Vivo NMR Research Center, National Center for Research Resources (C.T.W.M.), and the Laboratory of Diagnostic Radiology Research, Office of the Director (J.H.D.), National Institutes of Health, Bethesda, Md; and the Department of Radiological Sciences, University of California, Los Angeles (J.R.A.).

Address reprint requests to Giovanni Di Chiro, MD, Neuroimaging Branch, NINDS, NIH, Bldg 10, Room 1C227, 9002 Rockville Pike, Bethesda, MD 20892.

AJNR 17:1871–1879, Nov 1996 0195-6108/96/1710–1871

study was performed to assess the reproducibility of long-TE multisection proton MR spectroscopic imaging in healthy young adults. Our purpose was to study intraindividual, interindividual, interregional, and intraregional reproducibility.

## Materials and Methods

Six healthy subjects (30 to 40 years of age) participated in the study. Each subject underwent three proton MR spectroscopic imaging examinations. The interval between each study was not uniform, as one subject had two scans separated by 4 months and others by a few days. Informed consent was given under a human research protocol approved by the appropriate local authority. We used conventional MR images to reposition subjects during subsequent examinations as they were positioned in their initial examination and to select comparable anatomic regions of interest (ROIs) in all studies.

### *Proton MR Spectroscopic Imaging*

Proton MR spectroscopic imaging was performed on a 1.5-T MR imager equipped with self-shielded gradients (GE Medical Systems, Milwaukee, Wis) and standard quadrature imaging head coil, using a previously described data acquisition procedure (4). Section selection was performed with a spin-echo sequence with 2200/272 (repetition time/echo time). The section thickness was 15 mm and a 3-mm gap was used. Water suppression was achieved with a chemical-shift selective saturation pulse, and scalp lipids were suppressed by octagonal outer volume suppression. Circular phase encoding was performed to generate a $32 \times 32$ k-space matrix using a $24 \times 24$-cm field of view, which resulted in a nominal voxel size of $7.5 \times 7.5 \times 15$ mm.

The raw data from each section consisted of a set of 804 phase-encoded full spin echoes. The phase encodings sampled a circular region of the k-space centered at the origin. Each echo consisted of 256 complex points sampled 1 millisecond apart (sweep width = 1 kHz). The echoes were apodized by multiplying the nth point by the factor $\sin(np/128)$ for $n < 64$; 1 for $64 \leq n \leq 192$; and $\sin[(256 - n)p/128]$ for $n > 192$. The echoes were zero-filled to 512 points and Fourier transformed to the frequency domain, the k-space data were zero-filled to a $32 \times 32$ square matrix, and a radial cosine filter was applied over 50% of the data (4).

To generate metabolite signal intensity images, we used the following procedure: first, the magnitude for each spectrum was computed and then an automated peak-picking program was used to identify the choline-containing compounds (Cho), creatine plus phosphocreatine (Cr), *N*-acetyl–containing compounds (NAA), with *N*-acetylaspartate as the prominent contributor, and lactate peaks. Then the peak identifications were reviewed and manually changed for any in which the automatic procedure had failed, and spectra from voxels contaminated by fat were zeroed out. After the peaks in all the spectra were properly identified, the metabolite values were determined for each pixel by summing the magnitude spectrum over a frequency bandwidth of 6 Hz (0.1 ppm) centered at each peak. The magnitude values were integrated to produce four $32 \times 32$ arrays showing spatial variation of the strength of each of the signals in each of the selected sections.

Conventional 3-mm-thick T1-weighted MR images, obtained immediately after the proton MR spectroscopic imaging acquisition, were used to identify the ROIs. The proton MR spectroscopic imaging signal magnitude images were imported into a Macintosh computer for anatomic comparison with the MR imaging data. ROIs containing an integral number of 0.84 $cm^3$ spectroscopic voxels were drawn on the T1-weighted MR images and then transferred to the identical location on all proton MR spectroscopic images to obtain the proton MR spectroscopic imaging signal intensities in these locations. The spectra of all voxels within the ROIs were examined manually. Only spectra from voxels that satisfied the following criteria were included in the subsequent analysis: 1) the voxel boundaries traced on each of the five 3-mm-thick MR sections that correspond to the 15-mm-thick proton MR spectroscopic imaging sections were entirely within the anatomic ROI; 2) the low point between the Cho and Cr signal was below the half-width of the smaller of the two signals; 3) the baseline in the Cho and Cr region was flat and centered at the origin of the y-axis of the display; and 4) the baseline in the NAA region was flat and centered at the origin of the y-axis of the display. Criterion 1 served to eliminate spectra in which there was a contribution from multiple anatomic volumes so as to minimize partial volume effects. Criterion 2 served to eliminate spectra in which the integration procedure would erroneously include Cho intensity in the estimate of Cr intensity, and vice versa; it also served to guarantee that NAA signals would not be underestimated by the integration procedure because they were broad. Criteria 3 and 4 served to minimize the influence that poor water suppression or lipid contamination would have on the estimated signal intensities through raising and tilting the baseline.

Eight neuroanatomic ROIs were identified in gray matter, white matter, and subcortical nuclei. Gray matter ROIs were selected in the frontal cortex, occipital cortex, parietal cortex, insular cortex, and cingulate gyrus. White matter ROIs were selected in the centrum semiovale. Basal nuclei ROIs were selected in the thalamus and caudate. Since lack of significant side-to-side asymmetry for any of the metabolites in any of the ROIs evaluated was previously reported (1), values from bilateral ROIs in the present study were averaged together for statistical purposes.

Two methods were used to calibrate the signal intensities from the different subjects to a common scale: metabolite signal ratios were calculated from single ROIs (NAA/Cho, NAA/Cr, Cho/Cr); and the signal amplitude of each metabolite in each ROI was normalized to the correspond-

ing amplitude in the centrum semiovale (eg, NAA-thalamus/NAA-centrum semiovale). The centrum semiovale was used as a reference because it could be identified in each of the studies, and because its raw signal had previously shown the lowest coefficient of variation (CV) (1).

*Statistical Methods*

Statistical evaluation was performed by analyses of variance and components of variance method. In particular, the following statistical model was used for each metabolite ratio and centrum semiovale–normalized value (X): $X_{ijk} = \mu + S_i + V_{j(i)} + e_{ijk}$, where i = 1 to a (the number of subjects), j = 1 to b (the number of visits per individual), and k = 1 to n (the number of voxels per ROI). Here, $\mu$ denotes the overall mean, $S_i$ the effect due to subject i, $V_{j(i)}$ the effect of visit j nested in subject i, and e the error term. It is assumed that $S_i$, $V_{j(i)}$, and $e_{ijk}$ are all independent gaussian curves, with a mean of 0 and with variances of $\sigma_s^2$, $\sigma_v^2$, and $\sigma_e^2$, respectively. Here, the error variance is the variability due to multiple voxels within the same ROI. This is a measure of intraregional reproducibility and, as such, reflects the voxel variance as well as other variables associated with the measurements. The total variance of X, $\sigma_t^2$, is given by the sum of these three variance components: $\sigma_t^2 = \sigma_s^2 + \sigma_v^2 + \sigma_e^2$.

Components of variance methods are used to study the sources of variability by means of hypothesis testing and confidence interval estimation of variances and their ratios (5). In standard analysis of variance (ANOVA) terminology, the mean square error among subjects is an (unbiased) estimate of $bn\sigma_s^2 + n\sigma_v^2 + \sigma_e^2$, and the mean square error of visits within subjects is an estimate of $n\sigma_v^2 + \sigma_e^2$, where b is the number of visits per subject and n is the number of voxels per ROI. These two mean square errors are measures of interindividual and intraindividual reproducibility, respectively. The subject variance is then the difference of the mean squares between minus within, divided by bn. However, this difference, while on average is at least as large as zero, can sometimes be negative in a standard ANOVA. This is avoided by using a more sophisticated point estimation procedure called *restricted maximum likelihood estimation* (REML). In this application, the variance component analyses, using REML estimation of the metabolite ratios, were performed using the software package SAS (SAS Institute Inc, Cary, NC) (5). It is possible that some of the estimated variances for the components, while not less than zero, are zero under REML.

The (theoretical) CV is defined as the standard deviation $\sigma$ divided by the mean $\mu$: $CV = \sigma/\mu$. Therefore, dividing the above variance equation by the square of $\mu$ yields additivity in the squares of the CVs: $CV_t^2 = CV_s^2 + CV_v^2 + CV_e^2$, where the subscripts are as above and $\mu$ is estimated by the overall grand mean of, say, the ratios of NAA to Cr, and the various $\sigma^2$ by their REML estimates.

In order to investigate whether $CV_v$ and $CV_e$ differ for some ratio and ROI, confidence intervals are constructed for the ratio of the square of the $CV_s$ or equivalently for the ratio of the variance of visit to error. The $(1 - \alpha)$ 100% confidence interval for the variance ratio has lower and upper limits given in this case by $[(F/F_u) - 1]/n$ and $[(F - F_l) - 1]/n$, respectively, where F denotes the actual F ratio for the mean square visit divided by the mean square error from the ANOVA table and $F_l$ and $F_u$ are the lower $\alpha/2$ and upper $\alpha/2$ quantiles of the F distribution with $a(b - 1)$ and $ab(n - 1)$ degrees of freedom (6). For only a single ratio and a single ROI, one could use $\alpha = .05$. With the three ratios (NAA/Cho, NAA/Cr, Cho/Cr) in the eight ROIs, and the three centrum semiovale normalized values in the seven ROIs to adjust for the 24 + 21 = 45 separate inferences, a Bonferroni adjustment factor of 51 was used, resulting in an $\alpha = .05/45 = .0011$ for each inference. The quantiles of the F distribution are calculated by using the statistical software S-Plus (Stat SCI, Seattle, Wash). Each such confidence interval is examined to determine if 1 is outside the interval; that is, if 1 is either larger than the upper limit or less than the lower limit. If so, then there is evidence that the two variances and hence the two $CV_s$ differ for the ratio in that ROI.

The same method can be used to assist in the investigation of whether the $CV_s$ differs from $CV_v$. This is accomplished indirectly by forming confidence intervals for the ratio of $\sigma_s^2/(\sigma_v^2 + \sigma_e^2/n)$. This method uses the ratio F from the ANOVA table, calculated by dividing the mean square subject divided by the mean square error. This is the formula for the lower and upper limits of the $(1 - \alpha)$ 100% confidence interval for the ratio given by $[(F/F_u) - 1]/b$ and $[(F - F_l) - 1]/b$, where b (= 3) is the number of visits per subject and $F_l$ and $F_u$ are the lower $\alpha/2$ and upper $\alpha/2$ quantiles of the F distribution, with $a - 1 = 5$ and $(a - 1)b = 12$ degrees of freedom. If the lower limit exceeds 1, there is evidence that the subject variance is significantly larger than the visit variance. If the upper limit is less than 1, it is merely suggestive that the subject variance is smaller.

## Results

Figure 1 provides representative image data from the study. It shows MR images and proton MR spectroscopic images from three studies of one subject. The MR imaging section is 3 mm thick and corresponds to the center of the 15-mm-thick proton MR spectroscopic imaging section. Proton MR spectroscopic imaging data are displayed at their nominal voxel in-plane resolution (7.5 × 7.5 mm) using a color scale that depicts the strongest signal integral with red and the weakest with dark blue. Color images are scaled to the highest value of any of the metabolite signal intensities for each proton MR spectroscopic imaging section, so that the pattern of regional distribution of metabolite signal intensities within the same section can be compared among subjects, although color intensities from the same anatomic location can-

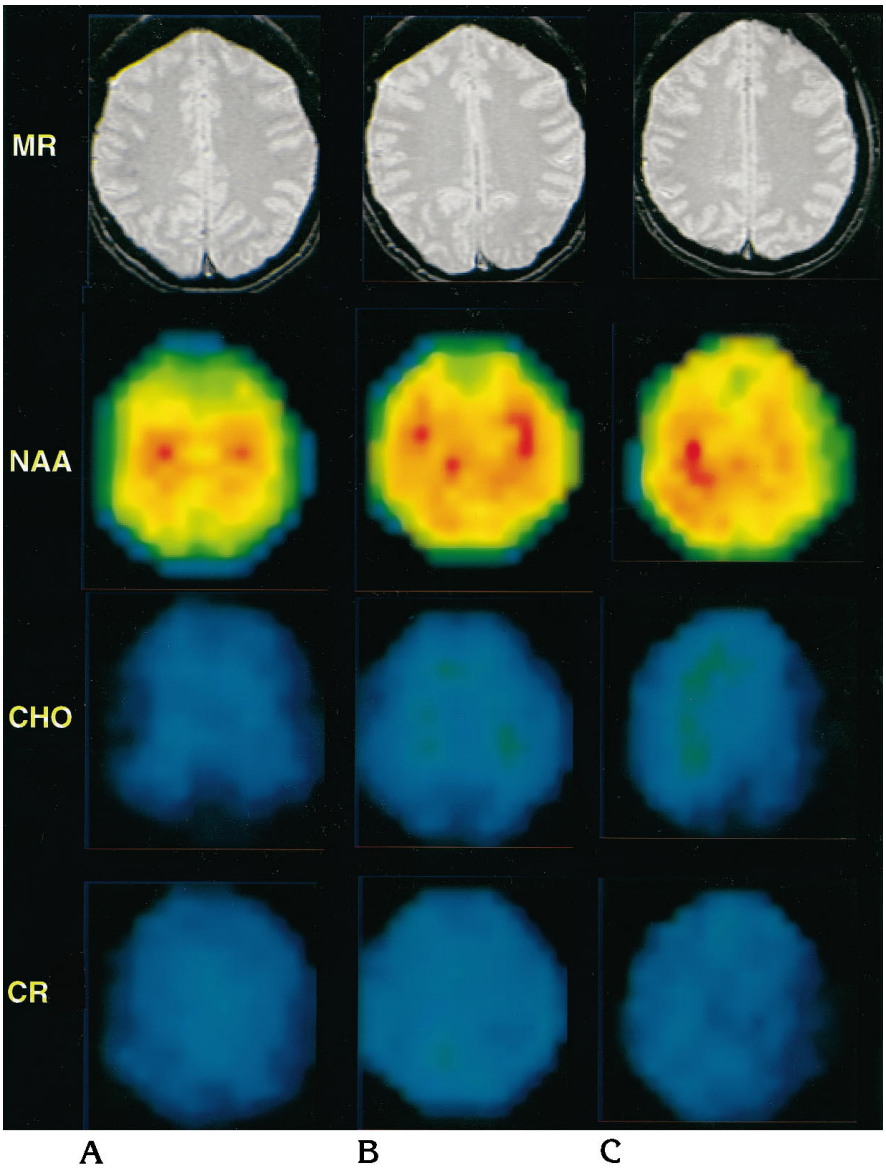


Fig 1. T1-weighted MR images and proton MR spectroscopic images of a subject on three repeated examinations (*A*, *B*, *C*, respectively) at one of the four possible section levels. The MR section is 3 mm thick and corresponds to the center of the 15-mm-thick proton MR spectroscopic imaging section.

not be compared among subjects. The three MR images show minor differences in section location despite the effort to reposition the subject at subsequent examinations.

Figure 2 shows the location of the selected ROIs in one subject, as well as some representative spectra.

Table 1 presents the overall mean values of measured ratio parameters for each of the ROIs. The values in the Table were obtained by calculating the average among subjects, visits, and voxels within each ROI. The mean number of voxels per scan was 6.0 for the centrum semiovale, frontal cortex, and insular cortex; 5.9 for the thalamus; 5.8 for the parietal cortex; 5.3 for the occipital cortex; 4.0 for the cingulate gyrus; and 1.9 for the caudate. The regional difference in number of voxels per scan is due to a combination of the size and location of the anatomic structure. The first limits the number of voxels that can fit into the five 3-mm-thick MR sections corresponding to the 15-mm-thick proton MR spectroscopic imaging section; the second limits the number of spectra that would fulfill the above-mentioned criteria and be suitable for proper analysis.

Table 1 also presents the overall standard deviation and CVs associated with the 18 mean observations. Each mean is obtained by averaging the voxels within each ROI for each visit of each person. These overall standard deviations and CVs reflect the combination of interindi-

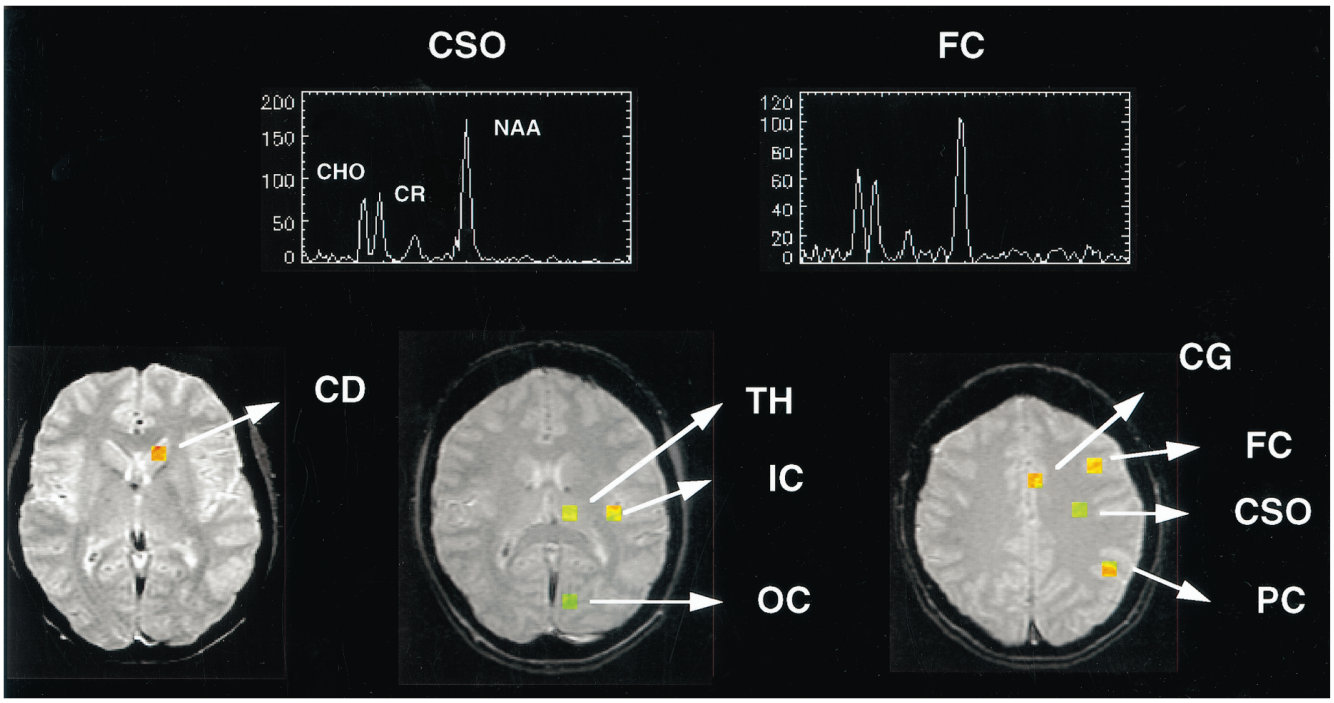


Fig 2. Representative spectra from white and gray matter and location of ROIs in one subject. *FC* indicates frontal cortex; *OC*, occipital cortex; *PC*, parietal cortex; *lC*, insular cortex; *CG*, cingulate gyrus; *CSO*, centrum semiovale; *TH*, thalamus; and *CD*, caudate.

vidual, intraindividual, and intraregional reproducibility. With respect to the metabolite signal intensity ratios: NAA/Cr showed the lowest CV in the centrum semiovale and a CV lower than 15% in all other ROIs except the caudate; NAA/Cho showed a CV lower than 20% only in the centrum semiovale and frontal cortex; Cho/Cr showed the lowest CV in the frontal cortex and centrum semiovale and a CV lower than 20% in all other ROIs except the occipital cortex and caudate. With respect to centrum semiovale–normalized values, NAA/centrum semiovale showed the lowest CV in the frontal cortex and cingulate gyrus and a CV lower than 20% in all other ROIs except the caudate; the Cho/centrum semiovale showed a CV lower than 20% in the frontal cortex, parietal cortex, occipital cortex, cingulate gyrus, and thalamus; the Cr/centrum semiovale showed a CV lower than 20% in the frontal cortex, parietal cortex, and cingulate gyrus.

Table 2 presents the total CV followed by the CVs for each of the three components (subject, visit, and voxel); each CV is a percentage of 100%. Note that the CVs of the three components do not generally add up to the total CV, but the squares of the CV do. The total CV is larger than the corresponding overall CV (Table 1), because here the variability within each ROI (the voxel component) is also studied. The CV of the subject was always smaller than that of the visit, except for NAA/Cho in the occipital cortex; Cho/Cr in the centrum semiovale, frontal cortex, and thalamus; NAA/centrum semiovale in the caudate; and Cho/centrum semiovale and Cr/centrum semiovale in the cingulate gyrus and caudate. The voxel CV was always larger than the subject and visit CVs except for NAA/Cr in the caudate; NAA/Cho in the occipital cortex, cingulate gyrus, and caudate; Cho/Cr in the occipital cortex, insular cortex, and caudate; NAA/centrum semiovale in the frontal cortex and insular cortex; Cho/centrum semiovale in the frontal cortex, occipital cortex, insular cortex, thalamus, and caudate; Cr/centrum semiovale in the parietal cortex, occipital cortex, insular cortex, thalamus, and caudate. The voxel CV was larger than the subject CV only in three cases: the Cho/centrum semiovale in the insular cortex and caudate and the Cr/centrum semiovale in the caudate.

There is no evidence after the Bonferroni adjustment that there are any differences in the variances from the method described above. For example, for the ratio Cho/Cr in the centrum semiovale, the CVs in Table 2 are 4.5% for visit and 14.7% for voxel, suggesting that the visit variance may be significantly smaller. The

**TABLE 1: Mean metabolite ratios, mean centrum semiovale–normalized metabolite values, and overall standard deviation (SD) and coefficient of variation (CV, %)**

| Region of Interest | NAA/Cr | | | NAA/Cho | | | Cho/Cr | | |
|---|---|---|---|---|---|---|---|---|---|
| | Mean | SD | CV | Mean | SD | CV | Mean | SD | CV |
| Centrum semiovale | 3.12 | 0.3 | 8.9 | 2.73 | 0.41 | 15.2 | 1.16 | 0.1 | 11.7 |
| Frontal cortex | 2.85 | 0.4 | 14.0 | 2.95 | 0.53 | 17.9 | 0.98 | 0.1 | 10.0 |
| Parietal cortex | 2.81 | 0.4 | 14.9 | 3.16 | 0.57 | 26.1 | 0.92 | 0.2 | 19.7 |
| Occipital cortex | 2.68 | 0.4 | 13.8 | 3.30 | 0.7 | 21.2 | 0.84 | 0.2 | 23.4 |
| Cingulate gyrus | 2.48 | 0.3 | 11.9 | 2.68 | 0.73 | 27.4 | 0.97 | 0.2 | 19.2 |
| Insular cortex | 2.51 | 0.3 | 12.4 | 2.28 | 0.61 | 26.8 | 1.14 | 0.2 | 15.5 |
| Thalamus | 2.54 | 0.3 | 12.7 | 2.04 | 0.45 | 21.9 | 1.29 | 0.3 | 19.2 |
| Caudate | 2.38 | 0.6 | 26.1 | 2.19 | 0.51 | 23.4 | 1.11 | 0.2 | 21.1 |
| | NAA/Centrum Semiovale | | | Cho/Centrum Semiovale | | | Cr/Centrum Semiovale | | |
| | Mean | SD | CV | Mean | SD | CV | Mean | SD | CV |
| Centrum semiovale | 1.00 | ... | ... | 1.00 | ... | ... | 1.00 | ... | ... |
| Frontal cortex | 0.75 | 0.07 | 9.3 | 0.70 | 0.1 | 14.5 | 0.83 | 0.1 | 16.6 |
| Parietal cortex | 0.71 | 0.11 | 15.8 | 0.63 | 0.13 | 19.9 | 0.81 | 0.16 | 19.9 |
| Occipital cortex | 0.84 | 0.13 | 15.7 | 0.71 | 0.12 | 17.3 | 1.00 | 0.2 | 20.4 |
| Cingulate gyrus | 0.86 | 0.08 | 9.2 | 0.91 | 0.14 | 15.9 | 1.09 | 0.12 | 10.6 |
| Insular cortex | 0.79 | 0.16 | 19.9 | 0.98 | 0.28 | 28.4 | 0.99 | 0.22 | 22.7 |
| Thalamus | 0.78 | 0.14 | 17.7 | 1.05 | 0.17 | 15.9 | 0.98 | 0.23 | 23.6 |
| Caudate | 0.63 | 0.16 | 25.8 | 0.80 | 0.24 | 29.5 | 0.86 | 0.28 | 32.7 |

value of F that is the ratio of mean square (visit) to mean square voxel is 1.57, so the Bonferroni-adjusted 99.9% (actually, 99.89%) confidence interval has an upper boundary of 1.49, which is larger than 1. Hence, there is no evidence that the two variances differ in this case. If one were to construct the 99% confidence interval, the upper limit is 0.893, which is less than 1. If one were operating at level $\alpha = .01$, one would conclude that the visit variance is less than the voxel variance. In fact, even at $\alpha = .01$, of the 45 confidence intervals for the ratio of the variances, only two did not contain 1 (the other was Cho/Cr in the frontal cortex).

No lactate signals were found in any ROI. This finding is consistent with the normal intracerebral lactate concentration of approximately 0.5 $\mu$mol/g, which is close to or below the detection limit of the method we used.

## Discussion

Proton MR spectroscopy has evolved from single-volume localized proton MR spectroscopy to multisection proton MR spectroscopic imaging that permits simultaneous acquisition of metabolite signal intensities from four 15-mm-thick sections divided into 0.84-mL single-volume elements. Proton MR spectroscopic imaging is emerging as a tool for noninvasive studies of cerebral metabolites in a number of brain disorders (7–12). The principal metabolite signals on proton MR spectroscopic imaging, at a long TE, are NAA, Cho, Cr, and lactate. NAA is inferred to be a neuron-specific molecule because it is absent in both mature glial cell cultures and tumors of glial cell origin (13, 14). Moreover, immunofluorescence studies have shown that fluorescent anti-NAA antibodies colocalize with antibodies against neuron-specific proteins (15). The Cho peak reflects total brain choline stores (16), with major contribution from glycerophosphocholine and phosphocholine (17). The Cr peak reflects the total amount of phosphocreatine and creatine, which are involved in energy metabolism (16). Lactate signal rises whenever the glycolytic rate exceeds the capacity of oxidative metabolism or, possibly, when the capacity for exporting lactate to the bloodstream is impaired (18).

In a few studies (7, 8, 19), proton MR spectroscopy and proton MR spectroscopic imaging were used to assess the course of the disease and the effect of therapy. Bizzi et al (8) studied the early and long-term response to radiation therapy in a patient with central nervous system non-Hodgkin lymphoma by proton MR spectroscopic imaging. Barker et al (7) studied the evolution of acute stroke with serial proton MR spectroscopic imaging in a patient during a pe-

**TABLE 2: Coefficient of variation (%) of the total metabolite ratios and centrum semiovale–normalized ratios broken down into subject, visit, and voxel components by using variances as calculated by restricted maximum likelihood estimation**

| Region of Interest | NAA/Cr | | | | NAA/Cho | | | | Cho/Cr | | | |
|---|---|---|---|---|---|---|---|---|---|---|---|---|
| | Total | Subject | Visit | Voxel | Total | Subject | Visit | Voxel | Total | Subject | Visit | Voxel |
| Centrum semiovale | 18.2 | 0.0 | 8.4 | 16.2 | 19.5 | 6.8 | 12.8 | 13.0 | 18.4 | 10.1 | 4.5 | 14.7 |
| Frontal cortex | 19.3 | 4.2 | 12.0 | 14.5 | 24.7 | 7.5 | 16.2 | 17.1 | 17.9 | 6.8 | 4.6 | 15.9 |
| Parietal cortex | 25.1 | 5.0 | 12.4 | 21.2 | 31.7 | 8.5 | 22.8 | 20.4 | 23.6 | 5.0 | 16.6 | 16.0 |
| Occipital cortex | 20.5 | 6.9 | 11.6 | 15.4 | 26.8 | 15.7 | 13.9 | 16.7 | 30.5 | 11.7 | 21.0 | 18.8 |
| Cingulate gyrus | 15.3 | 3.8 | 8.2 | 12.3 | 31.0 | 7.6 | 25.8 | 15.5 | 23.5 | 11.4 | 14.4 | 14.6 |
| Insular cortex | 19.2 | 5.7 | 10.0 | 15.4 | 33.0 | 17.4 | 21.5 | 17.9 | 19.8 | 9.2 | 12.5 | 12.2 |
| Thalamus | 20.7 | 4.2 | 10.1 | 17.6 | 22.1 | 13.8 | 16.2 | 16.8 | 26.9 | 13.6 | 13.4 | 18.9 |
| Caudate | 31.3 | 8.7 | 22.2 | 20.3 | 24.7 | 0.0 | 19.6 | 14.9 | 23.2 | 4.4 | 18.9 | 12.6 |
| | NAA/Centrum Semiovale | | | | Cho/Centrum Semiovale | | | | Cr/Centrum Semiovale | | | |
| | Total | Subject | Visit | Voxel | Total | Subject | Visit | Voxel | Total | Subject | Visit | Voxel |
| Frontal cortex | 17.8 | 0.0 | 10.0 | 14.7 | 24.3 | 0.0 | 13.5 | 20.2 | 23.5 | 5.6 | 14.6 | 17.6 |
| Parietal cortex | 20.6 | 0.0 | 14.7 | 14.4 | 27.2 | 9.9 | 15.8 | 20.9 | 25.7 | 0.0 | 18.2 | 18.1 |
| Occipital cortex | 18.5 | 4.4 | 14.1 | 11.1 | 20.8 | 0.0 | 15.8 | 13.5 | 22.6 | 0.0 | 18.5 | 12.6 |
| Cingulate gyrus | 12.1 | 5.3 | 7.2 | 8.2 | 17.4 | 7.0 | 12.2 | 10.3 | 14.5 | 6.4 | 5.8 | 11.6 |
| Insular cortex | 21.8 | 9.5 | 16.7 | 10.5 | 33.1 | 23.3 | 15.8 | 17.4 | 25.6 | 13.2 | 16.9 | 14.0 |
| Thalamus | 23.3 | 10.2 | 13.7 | 15.9 | 19.4 | 10.9 | 11.8 | 11.0 | 29.1 | 13.6 | 19.0 | 17.4 |
| Caudate | 29.5 | 16.6 | 14.7 | 19.5 | 32.4 | 23.6 | 15.6 | 15.7 | 36.7 | 29.7 | 6.5 | 20.5 |

riod of 3 hours to 5 months after symptom onset. In both these studies, comparison of data from different studies was accomplished by measuring the signal intensities of each metabolite in the lesion and in the same location in the contralateral hemisphere. Vion-Dury et al (19) studied three patients with acquired immunodeficiency syndrome dementia complex by single-volume proton MR spectroscopy with the ROI positioned in the same parietooccipital white matter area in two consecutive examinations done before and after treatment with zidovudine. In this work, absolute intensities of NAA, Cho, and Cr signals were calculated by multiplying the area of resonances by the actual reference pulse amplitude, which was used as an internal calibration.

As proton MR spectroscopy and proton MR spectroscopic imaging are used more extensively in the clinical environment to assess disease progression and, eventually, the effects of therapy, the reproducibility of proton MR spectroscopic imaging data in healthy control subjects becomes a crucial issue. Indeed, only after establishing the variability peculiar to the technique (in control subjects) can one accurately address the issue of variability due to disease. Furthermore, since it has been previously reported that metabolite signal intensities show a significant regional distribution pattern in healthy control subjects (1), it seems appropriate to assess the variability of proton MR spectroscopic imaging on a regional basis. Two previous studies have focused on the reproducibility of proton MR spectroscopy (2) and proton MR spectroscopic imaging (3). Narayana et al (2) studied the repeatability of single-volume long-TE proton MR spectroscopy. Their ROI was located in the frontal lobe and had a size of 27 $cm^3$, which would include both frontal white matter and frontal cortex. The CVs, as reported by Jackson et al (3), are 36% for NAA/Cr and 39% for Cho/Cr. In the present study, we measured only the frontal cortex and found its overall CV was 14.0% for NAA/Cr and 10.0% for Cho/Cr. Jackson et al (3) studied the reproducibility of short-TE proton MR spectroscopic imaging with a single-section technique from voxels located above the corpus callosum that would correspond to our centrum semiovale. The overall CV was 17.5% for NAA/Cr and 16.0% for Cho/Cr. In the present study, in the centrum semiovale, the overall CV was 8.9% for NAA/Cr and 11.7% for Cho/Cr. It is notable that the present proton MR spectroscopic imaging measurements have a better reproducibility than single-volume proton MR spectroscopic measurements, although it is not possible to explore intraregional reproducibility for the latter.

The present study assessed the reproducibility of proton MR spectroscopic imaging from several neuroanatomic locations and evaluated interindividual, intraindividual, and intra-

regional contributions to the CV. The most evident result was that NAA/Cr almost always showed the best overall CV of the three ratios (six of eight), and that the CV of Cho/Cr was usually smaller than the one of NAA/Cho (Table 1). This is consistent with the previously described relatively uniform distribution of Cr signal intensities through the brain (1) and suggests that, when metabolite signal intensity ratios have to be used to measure changes in NAA, the ratio NAA/Cr is preferred over NAA/Cho. For the centrum semiovale–normalized values, NAA/centrum semiovale usually showed the lowest overall CV of the other two metabolites (seven of eight), whereas Cho/centrum semiovale and Cr/centrum semiovale behaved in a similar fashion. As previously proposed (1), the centrum semiovale–normalized values offer a complementary way of assessing brain abnormalities by proton MR spectroscopic imaging that could be particularly valuable when all metabolite signal intensities are reduced by the pathologic process. This approach requires that the centrum semiovale must not be involved in the disease. The present findings provide additional evidence of the feasibility of this approach, since for several ROIs the centrum semiovale–normalized values (in particular NAA/centrum semiovale) showed an overall CV that was very close to the ones found with the metabolite ratios.

Another interesting result is the observation of regional differences in the overall CV for all the proton MR spectroscopic imaging values (Table 1). The regional differences in overall CV depend on the two inclusion criteria followed to select ROIs. First, the size of the anatomic structure influences the number of spectroscopic voxels that could be selected; this, in turn, influences the CV. Indeed, the ROI with the smallest mean number of voxels per study (caudate) showed the highest CV in most of the proton MR spectroscopic imaging values, while the ROI with the highest mean number of voxels per study (centrum semiovale) showed the lowest CV in most of the proton MR spectroscopic imaging values. Second, the quality of the spectra depends on the location of the anatomic region. Some regions (ie, the frontal lobes and the posterior fossa structures) could have partial $B_o$ inhomogeneity due to the proximity of sinuses and bones. In some cases, the outer-volume saturation procedure did not completely eliminate contamination of the more superficial ROI spectra with signals arising from skull marrow and surface tissues. In regions near the ventricles, $B_o$ inhomogeneity could led to broadened Cho and Cr signals, which may be difficult to separate. Furthermore, the $B_o$ inhomogeneity in these regions in combination with the long T2 of cerebrospinal fluid results in suboptimal suppression of the water signal, which complicates baseline assignment in the Cho-Cr spectral region, thereby reducing the precision and accuracy of signal integration. These findings highlight the need for assessing the reproducibility of proton MR spectroscopy and proton MR spectroscopic imaging for the specific anatomic structure under investigation before using this technique for follow-up studies of brain disorders.

There are several comments relevant to the methodology for investigating differences in the variances and, hence, the CV. First, the approach is based on the assumption that the error structure is gaussian. If this assumption is not satisfied, the inference is not robust and may not be valid. Second, the resulting intervals are generally quite broad. This is a direct result of the fact that the study involves only six subjects, each imaged three times, and that a number of ratios and ROIs are being investigated. As the number of subjects or imaging visits per subject is increased and/or as the search is narrowed, these intervals will become more precise. Third, there are important implications arising from the understanding of the sources or components of variance. Although no significant differences between the three components of variance were found for any ROI, the voxel component often showed the highest value. However, it is likely that the most relevant source of variability was the tissue homogeneity in the ROI. If the voxels within an ROI are fairly homogeneous, it could be advantageous to collect the metabolite ratios in several voxels in order to estimate the overall level within the ROI more precisely. Further, the relationship between the subject and visit variance will prove quite helpful in designing experiments to distinguish between patients and healthy volunteers by means of metabolite ratios.

Despite the advantages of multisection proton MR spectroscopic imaging, some caveats remain. Owing to the extensive folding of the thin cortical gray matter ribbon with white matter, cortical spectroscopic voxels, even of the order of 0.84 mL, may contain a mixture of both tissue types. Furthermore, because of cerebral

atrophy, some spectroscopic voxels could be contaminated with cerebrospinal fluid. However, even if a markedly greater amount of cerebrospinal fluid were present in some selected ROIs, all metabolite signals would be equally decreased without affecting the metabolite ratios. We also anticipate that correcting proton MR spectroscopic imaging data for tissue composition, as assessed by the MR segmentation technique, could improve the accuracy of proton MR spectroscopic imaging to distinguish between gray matter and white matter abnormalities and could eventually result in a reduction of intraregional variability. Another potential confounding factor in an hour-long study is motion. We visually inspected the T1-weighted images before and after the proton MR spectroscopic imaging acquisition for evidence of motion and excluded studies of subjects who had obviously moved during the examination. We could not exclude more subtle motion artifacts.

Finally, the metabolite values found in the present study were different from those reported in a previous article concerning healthy adults (1). This is to be attributed to differences in spectroscopic inclusion criteria. Nevertheless, a Bonferroni analysis of the regional differences among the ROIs produced the same pattern as that previously reported (1). Thus, the present study confirms that there are significant differences in metabolite signal intensities among different ROIs in healthy adults.

## Acknowledgments

We thank J. L. Black and R. S. Hill for skillful technical assistance in performing the MR imaging and proton MR spectroscopic studies.

## References

1. Tedeschi G, Bertolino A, Righini A, et al. Brain regional distribution pattern of metabolite signal intensities in young adults by proton magnetic resonance spectroscopic imaging. *Neurology* 1995;45:1384–1391
2. Narayana PA, Johnston D, Flamig DP. In vivo proton magnetic resonance spectroscopy studies of human brain. *Magn Reson Imaging* 1991;9:303–308
3. Jackson EF, Doyle TJ, Wolinsky JS, Narayana PA. Short TE hydrogen-1 spectroscopic MR imaging of normal human brain: reproducibility studies. *J Magn Reson Imaging* 1994;4:545–551
4. Duyn JH, Gillen J, Sobering G, van Zijl PC, Moonen CTW. Multisection proton MR spectroscopic imaging of the brain. *Radiology* 1993;188:277–282
5. Snedecor GW, Cochran WG. *Statistical Methods*. 6th ed. Ames, Iowa: Iowa State University Press; 1967:285–288
6. Scheffe H. *The Analysis of Variance*. New York, NY: John Wiley & Sons; 1959:229–231
7. Barker PB, Gillard JH, van Zijl PCM, et al. Acute stroke: evaluation with serial proton MR spectroscopic imaging. *Radiology* 1994; 192:723–732
8. Bizzi A, Movsas B, Tedeschi G, et al. Response of non-Hodgkin lymphoma to radiation therapy: early and long-term assessment with H-1 MR spectroscopic imaging. *Radiology* 1995;194:271–276
9. Tedeschi G, Schiffmann R, Shih H H-L, et al. Proton magnetic resonance spectroscopic imaging in childhood ataxia with diffuse white matter hypomyelination. *Neurology* 1995;45:1526–1532
10. Kruse B, Barker PB, van Zijl PCM, et al. Multislice proton magnetic resonance spectroscopic imaging in X-linked adrenoleukodystrophy. *Ann Neurol* 1994;36:595–608
11. Tedeschi G, Bertolino A, Massaquoi SG, et al. Proton magnetic resonance spectroscopic imaging in cerebellar degeneration. *Ann Neurol* 1996;39:71–78
12. Barker PB, Lee RR, McArthur JC. AIDS dementia complex: evaluation with proton MR spectroscopic imaging. *Radiology* 1995; 195:58–64
13. Birken DL, Oldendorf WH. *N*-acetyl-L-aspartic acid: a literature review of a compound prominent in 1H-NMR spectroscopic studies of brain. *Neurosci Biobehav Rev* 1989;13:23–31
14. Urenjak J, Williams SR, Gadian DG, Noble M. Proton nuclear magnetic resonance spectroscopy unambiguously identifies different neural cell types. *J Neurosci* 1993;13:981–989
15. Moffett JR, Namboodiri MA, Cangro CB, Neale JH. Immunohistochemical localization of *N*-acetylaspartate in rat brain. *Neuroreport* 1991;2:131–134
16. Miller BL. A review of chemical issues in 1H NMR spectroscopy: *N*-acetylaspartate, creatine and choline. *NMR Biomed* 1991;4: 47–52
17. Barker PB, Breiter SN, Soher BJ, et al. Quantitative proton spectroscopy of canine brain: in vivo and in vitro correlations. *Magn Reson Med* 1994;32:157–163
18. Prichard J. What the clinician can learn from MRS lactate measurement. *NMR Biomed* 1991;4:99–102
19. Vion-Dury J, Nicoli F, Salvan AM, Confort-Gouny S, Dhiver C, Cozzone PJ. Reversal of brain metabolic alterations with zidovudine detected by proton localized magnetic resonance spectroscopy. *Lancet* 1995;345:60–61